Applied Physics Letters

Thermal conductivity of the $n = 1–5$ and 10 members of the $(SrTiO_3)_nSrO$ Ruddlesden–Popper superlattices

Cite as: Appl. Phys. Lett. **118**, 091904 (2021); https://doi.org/10.1063/5.0037765
Submitted: 16 November 2020 • Accepted: 06 February 2021 • Published Online: 04 March 2021

Natalie M. Dawley, Ella K. Pek, Che-Hui Lee, et al.

Applied Physics Letters ARTICLE scitation.org/journal/apl

Thermal conductivity of the $n = 1$–5 and 10 members of the $(SrTiO_3)_nSrO$ Ruddlesden–Popper superlattices

Cite as: Appl. Phys. Lett. **118**, 091904 (2021); doi: 10.1063/5.0037765
Submitted: 16 November 2020 · Accepted: 6 February 2021 ·
Published Online: 4 March 2021

View Online Export Citation CrossMark

Natalie M. Dawley,[1] Ella K. Pek,[2] Che-Hui Lee,[1] Eugene J. Ragasa,[3] Xue Xiong,[3,4,5] Kiyoung Lee,[6] Simon R. Phillpot,[3] Aleksandr V. Chernatynskiy,[7] David G. Cahill,[2] and Darrell G. Schlom[1,8,9,a)]

AFFILIATIONS

[1]Department of Materials Science and Engineering, Cornell University, Ithaca, New York 14853, USA
[2]Department of Materials Science and Engineering and Materials Research Laboratory University of Illinois at Urbana-Champaign, Urbana, Illinois 61801, USA
[3]Department of Materials Science and Engineering, University of Florida, Gainesville, Florida, 32611, USA
[4]Institute of Engineering Thermophysics, Chinese Academy of Sciences, Beijing 100190, China
[5]University of Chinese Academy of Sciences, Beijing 100049, China
[6]Inorganic Material Lab, Samsung Advanced Institute of Technology (SAIT), Samsung Electronics, 130 Samsung-ro, Yeongtong-gu, Suwon-si, Gyeonggi-do 16678, South Korea
[7]Department of Physics, Missouri University of Science and Technology, Rolla, Missouri 65409, USA
[8]Kavli Institute at Cornell for Nanoscale Science, Ithaca, New York 14853, USA
[9]Leibniz-Institut für Kristallzüchtung, 12489 Berlin, Germany

[a)]**Author to whom correspondence should be addressed:** schlom@cornell.edu

ABSTRACT

Unlike many superlattice structures, Ruddlesden–Popper phases have atomically abrupt interfaces useful for interrogating how periodic atomic layers affect thermal properties. Here, we measure the thermal conductivity in thin films of the $n = 1$–5 and 10 members of the $(SrTiO_3)_nSrO$ Ruddlesden–Popper superlattices grown by molecular-beam epitaxy and compare the results to a single crystal of the $n = 1$ Ruddlesden–Popper $SrLaAlO_4$. The thermal conductivity cross-plane to the superlattice layering (k_{33}) is measured using time-domain thermoreflectance as a function of temperature and the results are compared to first-principles calculations. The thermal conductivity of this homologous series decreases with increasing interface density. Characterization by x-ray diffraction and scanning transmission electron microscopy confirms that these samples have a Ruddlesden–Popper superlattice structure.

Materials with low thermal conductivity are of interest for a variety of applications including thermal barrier coatings[1,2] and thermoelectric devices.[3–5] Reducing dimensionality has been considered a promising approach to increase the effectiveness of a thermoelectric material.[4] As the dimensionality of a material is decreased, quantum-confinement effects begin to affect material properties, providing an additional variable to control material properties. Quantum well systems[6,7] and superlattices[8,9] have been investigated to lower thermal conductivity by reducing dimensionality through the addition of internal epitaxial interfaces. An outstanding challenge in these layered materials is the quality of their interfaces, which can suffer from internal surface roughness due to diffusion. The lack of atomically smooth interfaces can prevent accurate interpretation of a sample's thermal conductivity when compared to theoretical models. The $(SrTiO_3)_nSrO$ system we study in this Letter for its thermal conductivity properties naturally has atomically abrupt and smooth layers of $(SrO)_2$ inserted into $SrTiO_3$ as these superlattice materials are stable in bulk form as the Ruddlesden–Popper phases for $n = 1$–3.[10–13]

Several factors reduce thermal conductivity in superlattice structures. In general, internal interfaces inhibit the flow of heat. Across interfaces between dissimilar materials, differences in elastic properties impede the transfer of vibrational energy.[14] Theoretical calculations

show that the average phonon velocity decreases with increasing superlattice period due to increased phonon band folding.[15] Anharmonic phonon scattering due to the Umklapp process requires less energy in superlattices relative to the parent bulk materials due to a smaller reciprocal-lattice vector.[16] These properties have been well studied experimentally in synthetic semiconductor superlattices of GaAs–AlAs for their unique thermal conductivity[17,18] and phonon transport.[19] In this system, the conductivity measured in the in-plane direction was found to decrease with reducing superlattice period[17] and an even stronger reduction was found in the cross-plane direction (perpendicular to the layering).[18] As an analog system to the semiconductor superlattices, oxide superlattices show potential for thermoelectric applications.[20]

In this work, we report an experimental study on the thermal properties of a broad spectrum ($n = 1$–5 and 10) of $(SrTiO_3)_nSrO$ epitaxial films measured by the time-domain thermoreflectance (TDTR) technique.[3] The thermal conductivity of this homologous series shows decreasing thermal conductivity with n and is compared to first-principles calculations; the results of these first-principles calculations are consistent with those of our earlier analysis using empirical potentials.[21] $(SrTiO_3)_nSrO$ Ruddlesden–Popper phases have drawn extensive attention due to their potential applications as tunable dielectrics[22,23] and thermoelectric materials.[24] A similar system of the structurally related Dion–Jacobson homologous series, $A[A'_{n-1}B_nO_{3n+1}]$, was found to have an ultralow thermal conductivity ($\sim$0.4 W m^{-1} K^{-1}) in $CsBiNb_2O_7$,[25] the $n = 2$ member. $(SrTiO_3)_nSrO$ Ruddlesden–Popper phases have similar structural features; these natural superlattices are composed of an alternate stacking of double layers of rock salt SrO and n layers of perovskite $SrTiO_3$ along the c-axis, Fig. 1(b). With decreasing n, the repeat distance between inserted additional SrO layers decreases and the structure undergoes a transition from a two-dimensional interfacial system to a three-

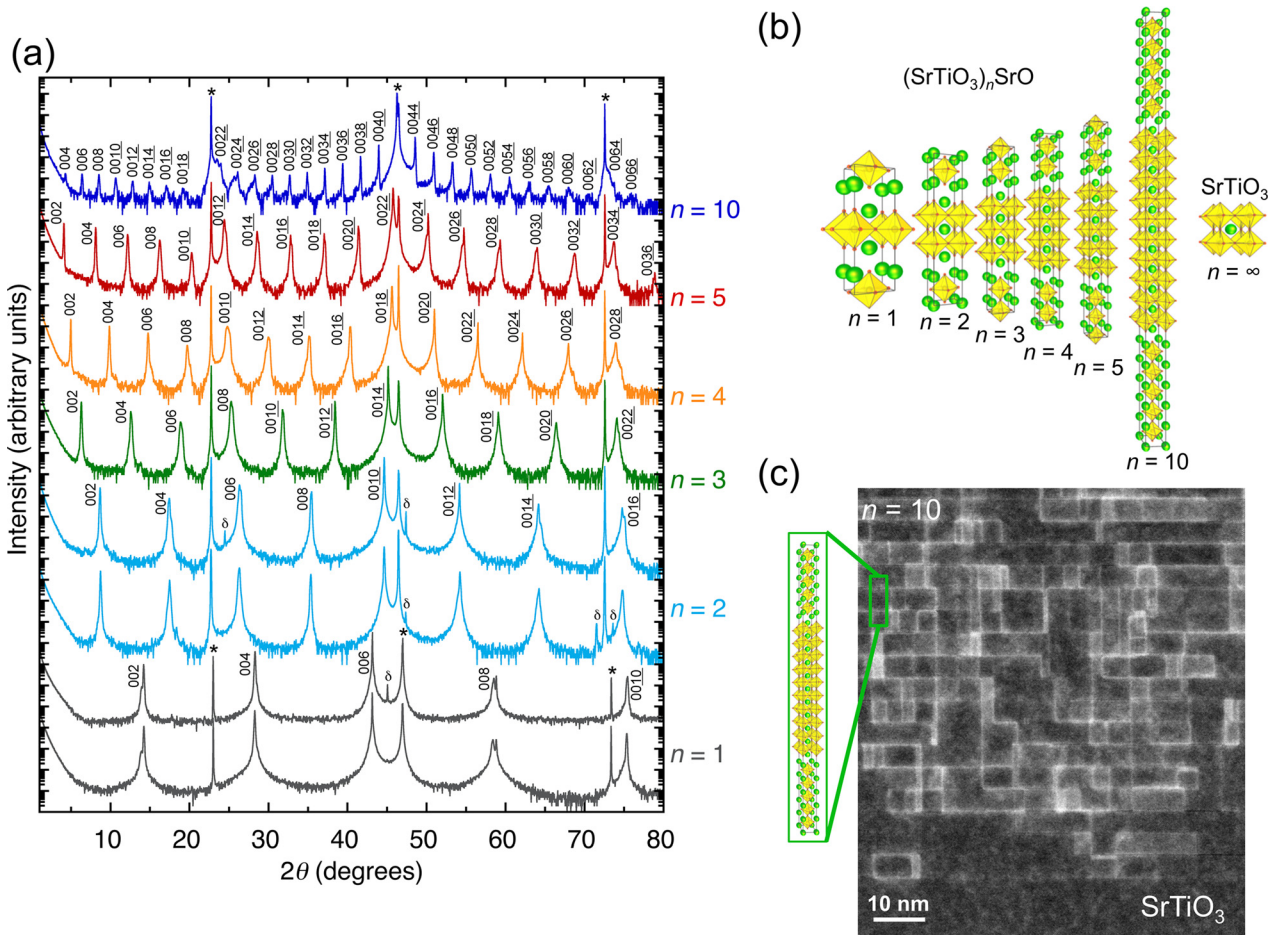

FIG. 1. (a) θ–2θ x-ray diffraction scans of 300-nm-thick epitaxial $(SrTiO_3)_nSrO$ films grown on (001) $SrTiO_3$ for $n = 2$–5 and 10 and 200-nm-thick films grown on (001) LSAT for $n = 1$. Substrate peaks are labeled with a (∗), and the plots are offset for clarity. Peaks labeled "δ" denote hybrid diffraction peaks (see Ref. 39). (b) Schematic of the $(SrTiO_3)_nSrO$ series unit cells, $n = 1$–5, 10, and ∞, pure $SrTiO_3$. Strontium atoms are shown in green and the TiO_6 oxygen coordination octahedra around each titanium ion are shown in yellow. (c) Low-angle annular dark-field scanning transmission electron microscopy (LAADF-STEM) of the $n = 10$ $(SrTiO_3)_nSrO$ film. A schematic of the $n = 10$ unit cell is shown on the left side of the image.

dimensional monolithic single crystal. The investigation of this homologous series provides an opportunity to tailor the thermal properties through changing dimensionality.

The synthesis of single-crystal $(SrTiO_3)_nSrO$ Ruddlesden–Popper phases is a challenging task. Conventional solid-state reactions only yield polycrystalline $n = 1$–3 members[10–13] due to the thermodynamic degeneracy of the higher-n phases of the series.[26,27] Severe intergrowth of mixed-n phases is generally found in attempts to make higher n members.[28] Here, we use the precise layering ability of oxide molecular-beam epitaxy (MBE) to grow not only the first five but also $n = 10$ $(SrTiO_3)_nSrO$ single-phase epitaxial films of 300 nm thickness. Oxide MBE can supply incident species in any desired sequence with submonolayer composition control and essentially arbitrary n values can be synthesized even though nearby phases have similar formation energies.[26–32]

We used a Veeco GEN10 oxide MBE system to grow the $(SrTiO_3)_nSrO$ ($n = 1$–5 and 10) films. The majority of the films were grown to a thickness of ~300 nm onto (001) $SrTiO_3$ ($a = 3.905$ Å) substrates; further growth details can be found in the supplementary material. The lattice mismatch of the $(SrTiO_3)_nSrO$ ($n = 1$–5 and 10) series to (001) $SrTiO_3$ decreases monotonically with n, from 0.6% for $n = 1$ to about 0.01% for $n = 10$. The mismatch for $n > 2$ was estimated from the weighted average of the in-plane lattice constants of bulk $n = 2$ $Sr_3Ti_2O_7$ ($a = 3.9026$ Å)[33] and bulk $SrTiO_3$ ($a = 3.905$ Å).[34] Two $n = 1$ samples ($a = 3.883$ Å) of 200 nm thickness were grown on (001) $(LaAlO_3)_{0.29}(SrAl_{0.5}Ta_{0.5}O_3)_{0.71}$ (LSAT) ($a = 3.869$ Å) for better lattice match (−0.4% vs 0.6% on (001) $SrTiO_3$) to allow us to grow a large enough volume of material for the accurate TDTR measurement without contribution from the substrate or added defects from lattice relaxation due to epitaxial stress as well as to approximate the bulk Sr_2TiO_4 lattice.[35] The predicted thermal penetration depth of TDTR in Sr_2TiO_4 at room temperature is 203 nm, $d = \sqrt{\Lambda/(\pi C f)}$, where thermal conductivity, Λ, was measured to be 2.9 W/m K, the heat capacity, C, of Sr_2TiO_4 is 2.41 J/cm^3 K,[36] and the laser frequency, f, used in our TDTR experiments is 9.3 MHz.

The structural perfection of the $(SrTiO_3)_nSrO$ homologous series was examined by x-ray diffraction (XRD). Figure 1 shows θ–2θ scans of the 300-nm-thick $n = 2$–5 and 10 films on (001) $SrTiO_3$ and the 200-nm-thick $n = 1$ films on (001) LSAT. Scans of each sample show all peaks corresponding to phase-pure $(SrTiO_3)_nSrO$ ($n = 1$–5 and 10). X-ray rocking curves in ω confirm the high structural perfection of the films; the full width at half maximum (FWHM) of the $n = 1$–5 and 10 films is less than 52 arc sec (<0.014°), comparable to the rocking curve FWHM of the 002 peak of the $SrTiO_3$ substrates themselves (see the supplementary material, Fig. S1). Sample quality affects thermal conductivity from the addition of phonon-scattering defects. Multiple samples of $n = 1$ and 2 are shown here to demonstrate how small variations in superlattice quality affect the trend in thermal conductivity in both interface density and temperature. The $n = 10$ $(SrTiO_3)_nSrO$ thin film was examined by low-angle annular dark field scanning transmission electron microscopy (LAADF-STEM); a micrograph is shown in Fig. 1(c). The film has the expected Ruddlesden–Popper structure with the larger atomically spaced $(SrO)_2$ layers appearing bright as compared to the surrounding $SrTiO_3$. The film also shows vertical $(SrO)_2$ intergrowths and projections through the sample seen as bright vertical lines and patches, respectively, forming a brick and mortar, patchwork structure of bulk $SrTiO_3$ and $(SrO)_2$ planes due to the low energy of formation of $(SrO)_2$ in $SrTiO_3$.[30,37,38]

Cross-plane thermal conductivity (k_{33}) of the entire series of $(SrTiO_3)_nSrO$ ($n = 1$–5 and 10) films was measured by TDTR.[40,41] TDTR is a non-contact, pump-probe optical technique that can be used for measuring thermal properties of materials on nanometer length scales. In our implementation of TDTR, a thin aluminum layer is deposited on the surface of the thin film and is pumped with a short pulse of a 9.8 MHz laser beam. A small fraction of energy from each pulse in the pump beam produces a sudden temperature jump of ~3 K near the surface of a sample. Decay of this near-surface temperature is then examined by the reflected energy of the pulses in the probe beam, i.e., the temperature change of the sample is measured by its temperature-dependent reflectance. The results of these time-resolved measurements are analyzed to obtain the cross-plane thermal conductivities. Further details of the TDTR measurements can be found in the supplementary material.

Figure 2(a) compares the thermal conductivities of the $(SrTiO_3)_nSrO$ phases acquired from TDTR measurements at room temperature to conductivities calculated from first-principles methods for the same temperature. The MBE syntheses and the atomic-level simulations were performed for six ($n = 1$–5 and 10) and four ($n = 1$–4) members, respectively, and reveal significant agreement in trends, minima, and magnitude of the thermal conductivity across the series. All samples show the expected trend of the conductivity decreasing with increasing density of thermal-resistant interfaces. Very similar trends, albeit with slightly larger values of thermal conductivity, were seen in the earlier empirical calculations of this system.[21] Phonons experience scattering at the interfaces between rock salt SrO and perovskite $SrTiO_3$ layers, which increases as n becomes smaller. For $n \leq 4$, the phonon mean free path is predicted to be larger than the spacing between the $(SrO)_2$ layers sandwiching $SrTiO_3$ [Fig. 2(a) inset]. A transition in the thermal conductivity, Fig. 2(a), and phonon mean free path, Fig. 2(a) inset, is predicted by our theoretical calculations for the $n = 1$ member as the system changes from being best represented as $SrTiO_3$ with SrO interfacial layers to a well-defined monolithic Ruddlesden–Popper crystal with its own phonon spectrum and thermal transport properties (Sr_2TiO_4). From the current experimental data, it is unclear if the $n = 1$ member has an increase in thermal conductivity as compared to $n = 2$.

A similar trend with interface density was observed in $SrTiO_3$-$BaTiO_3$ superlattice materials.[42] Compared to the perovskite-on-perovskite system, the Ruddlesden–Popper superlattices not only have an atomic-mass variation, but also a structural variation between superlattice layers from the perovskite slabs interleaved with rock salt-type SrO layers. Structural changes from layer-to-layer are believed to provide additional contributions to phonon scattering at the internal interfaces.

We used the VASP suite to carry out all the *ab initio* calculations shown in Fig. 2.[43–46] Full details of the calculations can be found in the supplementary material. In Fig. 2(b) at 300 K, excellent agreement between the *ab initio* calculations and experiment is observed for $SrTiO_3$, while the calculations slightly overpredict the measured thermal conductivity of the Ruddlesden–Popper phases. The disagreement might be related to the calculations having been carried out for the perfect structure, while measurements were performed on thin films with defects that are evident in Fig. 1(c).

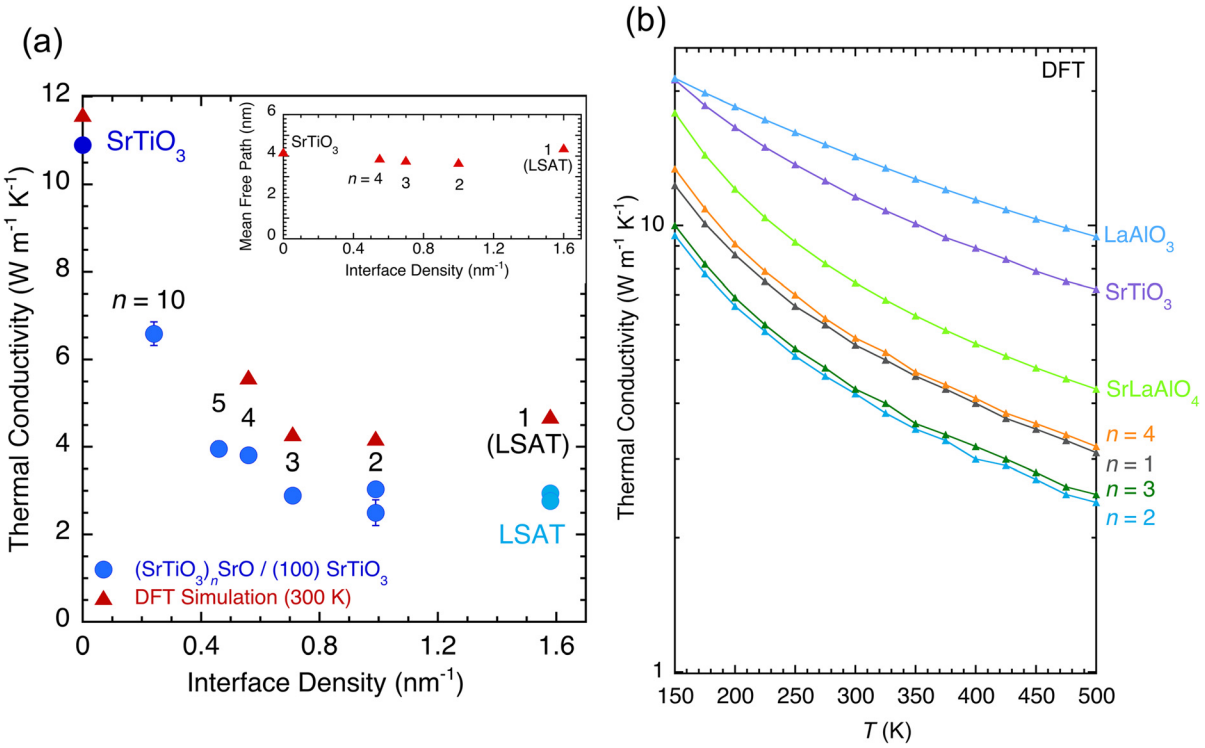

FIG. 2. (a) Summary of experimental and calculated cross-plane thermal conductivities (k_{33}) of the Ruddlesden–Popper $(SrTiO_3)_nSrO$ phases as a function of interface density at 300 K. The error bars of the experimental data taken at room temperature are the result of multiple measurements taken from different regions of the samples. To match our experimental series, the DFT simulation was performed for bulk $SrTiO_3$, and biaxial strained structures of $n = 1$–4 to replicate the epitaxial strain of the substrates used in our experiment, (001) $SrTiO_3$ or (001) LSAT. Inset: the phonon mean free path as calculated by DFT. (b) The *ab initio* calculated cross-plane thermal conductivities (k_{33}) of the Ruddlesden–Popper $(SrTiO_3)_nSrO$ phases, the Ruddlesden–Popper $SrLaAlO_4$, and its parent phase $LaAlO_3$ as a function of temperature.

The thermal conductivity was measured from 150 K to 500 K for all samples to investigate the temperature dependence of the thermal conductivity of superlattices with different interface densities. The experimental results are shown in Fig. 3(a). The thermal conductivities of $n = 1$–3 samples are relatively temperature independent. For $n = 4$, 5, and 10 samples, the slope of the thermal conductivities at higher temperatures approaches that of bulk $SrTiO_3$ with increasing n. To compare our thin film superlattices to a single crystal, samples of single crystal $SrLaAlO_4$, an $n = 1$ Ruddlesden–Popper, and its parent phase, $LaAlO_3$ (an $n = \infty$ Ruddlesden-Popper), were measured by TDTR from 150 K to 500 K. At room temperature, $SrLaAlO_4$ was observed to have a thermal conductivity of around 4 W m^{-1} K^{-1}. The *ab initio* calculation of k_{33} for $SrLaAlO_4$ is 7.4 W m^{-1} K^{-1} and for $LaAlO_3$, 14.3 W m^{-1} K^{-1}. The *ab initio* calculated values were found to be systematically higher when compared to the TDTR measurements. The measured thermal conductivity of our Sr_2TiO_4 films, 2.8–3 W m^{-1} K^{-1}, is significantly lower than the result of the *ab initio* calculations, 5.4 W m^{-1} K^{-1}, likely due to interface disorder in our MBE-grown films. The lack of perfect single-crystal quality is further confirmed when the temperature dependence of k_{33} of our Sr_2TiO_4 films is compared to that of single-crystal $SrLaAlO_4$. The two materials show a clear difference in trend, Fig. 3(b), indicating that our thin film samples have some atomic disorder possibly due to vertical $(SrO)_2$ faults,[22,36–38] flattening and lowering the temperature-dependent

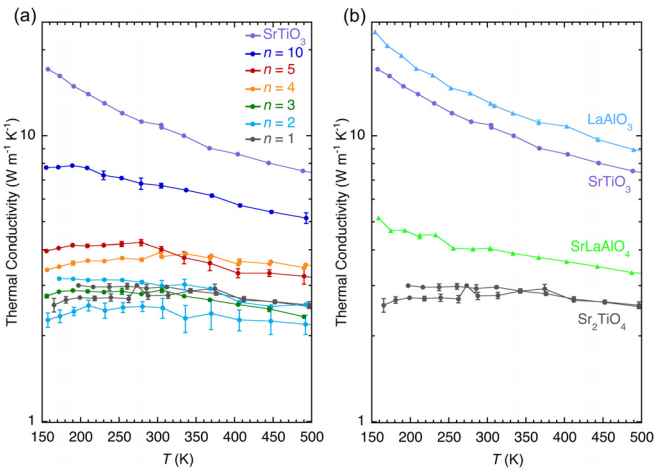

FIG. 3. (a) Experimental cross-plane thermal conductivities (k_{33}) of the Ruddlesden–Popper $(SrTiO_3)_nSrO$ phases measured from 500 K to 150 K. The error bars of the experimental data are the result of multiple measurements taken at different regions of the samples. (b) Comparison of experimentally measured k_{33} of $n = 1$ thin-film Sr_2TiO_4 with its parent ($n = \infty$) phase, a single crystal of $SrTiO_3$. Also shown is a comparison of the experimentally measured k_{33} of an $n = 1$ single-crystal $SrLaAlO_4$ and a single crystal of $LaAlO_3$ ($n = \infty$).

thermal conductivity. The temperature-dependence of the calculated and measured k_{33} of the Ruddlesden–Popper superlattices [a comparison between Figs. 2(b) and 3(a)] also shows that the thin films have a flatter temperature dependence than predicted by theory. The variance between our experimental results and theory improves at higher temperatures where defects dominate less of the phonon scattering as seen from the converging of the multiple $n = 1$ and 2 films with temperature in Fig. 3.

The investigation of this Ruddlesden–Popper series provides an opportunity to tailor the thermal properties through changing dimensionality. In this Letter, we summarize the experimental and theoretical thermal conductivity cross-plane to the superlattice layering of $(SrTiO_3)_nSrO$ phases as a function of interface density. The minimum in the temperature-dependent thermal conductivity as a function of n allows the thermal conductivity and its temperature dependence to be tuned. A transition in k_{33} at room-temperature is predicted but experimentally inconclusive for the $n = 1$ member as the distance between interfaces becomes smaller than the phonon mean free path. Intergrowths and planar faults in Ruddlesden–Popper phases likely serve as additional scattering centers and lower the effective phonon mean free path as compared to single crystal samples.

See the supplementary material for additional details on the $(SrTiO_3)_nSrO$ thin film growth and XRD characterization, the TDTR experimental setup, and further details of the *ab initio* calculations.

The synthesis and characterization work at Cornell was supported by the U.S. Department of Energy, Office of Basic Sciences, Division of Materials Sciences and Engineering, under Award No. DE-SC0002334. This work was sponsored by the Defense Advanced Research Projects Agency (DARPA) and the U.S. Army Aviation and Missile Research, Development, and Engineering Center (AMRDEC) under Contract No. W31P4Q-08-1-0012.[47] Support of the UCLA Center for Functional Engineered and Nano Architectonics is acknowledged. Sample preparation was in part facilitated by the Cornell NanoScale Facility, a member of the National Nanotechnology Coordinated Infrastructure (NNCI), which is supported by the National Science Foundation (Grant No. NNCI-2025233). This work made use of the Cornell Center for Materials Research Shared Facilities, which are supported through the NSF MRSEC program (No. DMR-1719875). This study was carried out in part in the Materials Research Laboratory Central Research Facilities, University of Illinois. This work was supported in part by the High Performance Computing Center at Missouri University of Science and Technology and by the National Science Foundation under Grant No. OAC-1919789.

DATA AVAILABILITY

The data that support the findings of this study are available in the supplementary material or from the corresponding author upon reasonable request.

REFERENCES

[1]N. P. Padture, M. Gell, and E. H. Jordan, Science **296**, 280 (2002).
[2]R. A. Miller, Surf. Coat. Technol. **30**, 1 (1987).
[3]Y. K. Koh, S. L. Singer, W. Kim, J. M. O. Zide, H. Lu, D. G. Cahill, A. Majumdar, and A. C. Gossard, J. Appl. Phys. **105**, 054303 (2009).
[4]M.-S. Dresselhaus, G. Chen, M.-Y. Tang, R.-G. Yang, H. Lee, D.-Z. Wang, Z.-F. Ren, J.-P. Fleurial, and P. Gogna, Adv. Mater. **19**, 1043 (2007).
[5]G. J. Snyder and E. S. Toberer, Nat. Mater. **7**, 105 (2008).
[6]T. C. Harman, P. J. Taylor, M. P. Walsh, and B. E. LaForge, Science **297**, 2229 (2002).
[7]T. C. Harman, M. P. Walsh, B. E. LaForge, and G. W. Turner, J. Electron. Mater. **34**, L19 (2005).
[8]R. Venkatasubramanian, Phys. Rev. B **61**, 3091 (2000).
[9]R. Venkatasubramanian, E. Siivola, T. Colpitts, and B. O'Quinn, Nature **413**, 597 (2001).
[10]D. Balz and K. Plieth, Z. Elektrochem. **59**, 545–551 (1955).
[11]S. N. Ruddlesden and P. Popper, Acta Crystallogr. **10**, 538–539 (1957).
[12]S. N. Ruddlesden and P. Popper, Acta Crystallogr. **11**, 54–55 (1958).
[13]G. J. McCarthy, W. B. White, and R. Roy, J. Am. Ceram. Soc. **52**, 463–467 (1969).
[14]G. Chen, Phys. Rev. B **57**, 14958 (1998).
[15]M. V. Simkin and G. D. Mahan, Phys. Rev. Lett. **84**, 927 (2000).
[16]W. S. Capinski, H. J. Maris, T. Ruf, M. Cardona, K. Ploog, and D. S. Katzer, Phys. Rev. B **59**, 8105 (1999).
[17]T. Yao, Appl. Phys. Lett. **51**, 1798 (1987).
[18]W. S. Capinski and H. J. Maris, Physica B **219–220**, 699 (1996).
[19]C. Colvard, T. A. Gant, M. V. Klein, R. Merlin, R. Fisher, H. Morkoc, and A. C. Gossard, Phys. Rev. B **31**, 2080 (1985).
[20]H. Ohta, S. Kim, Y. Mune, T. Mizoguchi, K. Nomura, S. Ohta, T. Nomura, Y. Nakanishi, Y. Ikuhara, M. Hirano, H. Hosono, and K. Koumoto, Nat. Mater. **6**, 129 (2007).
[21]A. Chernatynskiy, R. W. Grimes, M. A. Zurbuchen, D. R. Clarke, and S. R. Phillpot, Appl. Phys. Lett. **95**, 161906 (2009).
[22]C.-H. Lee, N. D. Orloff, T. Birol, Y. Zhu, V. Goian, E. Rocas, R. Haislmaier, E. Vlahos, J. A. Mundy, L. F. Kourkoutis, Y. Nie, M. D. Biegalski, J. Zhang, M. Bernhagen, N. A. Benedek, Y. Kim, J. D. Brock, R. Uecker, X. X. Xi, V. Gopalan, D. Nuzhnyy, S. Kamba, D. A. Muller, I. Takeuchi, J. C. Booth, C. J. Fennie, and D. G. Schlom, Nature **502**, 532 (2013).
[23]N. M. Dawley, E. J. Marksz, A. M. Hagerstrom, G. H. Olsen, M. E. Holtz, V. Goian, C. Kadlec, J. Zhang, X. Lu, J. A. Drisko, R. Uecker, S. Ganschow, C. J. Long, J. C. Booth, S. Kamba, C. J. Fennie, D. A. Muller, N. D. Orloff, and D. G. Schlom, Nat. Mater. **19**, 176–181 (2020).
[24]Y. Wang, K. H. Lee, H. Ohta, and K. Koumoto, J. Appl. Phys. **105**, 103701 (2009).
[25]D. G. Cahill, A. Melville, D. G. Schlom, and M. A. Zurbuchen, Appl. Phys. Lett. **96**, 121903 (2010).
[26]K. R. Udayakumar and A. N. Cormack, J. Amer. Ceram. Soc. **71**, C469 (1988).
[27]*The Chemistry of Extended Defects in Non-Metallic Solids: Proceedings of the Institute for Advanced Study on the Chemistry of Extended Defects in Non-Metallic Solids*, edited by L. Eyring and M. O'Keefe (North-Holland, Amsterdam, 1970), pp. 1–20.
[28]R. J. D. Tilley, J. Solid State Chem. **21**, 293–301 (1977).
[29]J. H. Haeni, C. D. Theis, D. G. Schlom, W. Tian, X. Q. Pan, H. Chang, I. Takeuchi, and X.-D. Xiang, Appl. Phys. Lett. **78**, 3292 (2001).
[30]W. Tian, X. Q. Pan, J. H. Haeni, and D. G. Schlom, J. Mater. Res. **16**, 2013 (2001).
[31]N. D. Orloff, W. Tian, C. J. Fennie, C.-H. Lee, D. Gu, J. Mateu, X. X. Xi, K. M. Rabe, D. G. Schlom, I. Takeuchi, and J. C. Booth, Appl. Phys. Lett. **94**, 042908 (2009).
[32]W. Tian, J. H. Haeni, D. G. Schlom, E. Hutchinson, B. L. Sheu, M. M. Rosario, P. Schiffer, Y. Liu, M. A. Zurbuchen, and X. Q. Pan, Appl. Phys. Lett. **90**, 022507 (2007).
[33]M. M. Elcombe, E. H. Kisi, K. D. Hawkins, T. J. White, P. Goodman, and S. Matheson, Acta Cryst. B **47**, 305 (1991).
[34]*Landolt-Börnstein: Numerical Data and Functional Relationships in Science and Technology New Series, Group III*, edited by K.-H. Hellwege and A. M. Hellwege (Springer, Berlin, 1979), Vol. 11, p. 418.
[35]B. C. Chakoumakos, D. G. Schlom, M. Urbanik, and J. Luine, J. Appl. Phys. **83**, 1979 (1998).
[36]K. T. Jacob and G. Rajitha, J. Chem. Thermodyn. **43**, 51 (2011).
[37]M. A. McCoy, R. W. Grimes, and W. E. Lee, Philos. Mag. A **75**, 833 (1997).
[38]T. Suzuki, Y. Nishi, and M. Fujimoto, Philos. Mag. A **80**, 621 (2000).

[39]E. H. Smith, P. D. C. King, A. Soukiassian, D. G. Ast, and D. G. Schlom, Appl. Phys. Lett. **111**, 131903 (2017).
[40]D. G. Cahill, W. K. Ford, K. E. Goodson, G. D. Mahan, A. Majumdar, H. J. Maris, R. Merlin, and S. R. Phillpot, J. Appl. Phys. **93**, 793 (2003).
[41]D. G. Cahill, Rev. Sci. Instrum. **75**, 5119 (2004).
[42]J. Ravichandran, A. K. Yadav, R. Cheaito, P. B. Rossen, A. Soukiassian, S. J. Suresha, J. C. Duda, B. M. Foley, C.-H. Lee, Y. Zhu, A. W. Lichtenberger, J. E. Moore, D. A. Muller, D. G. Schlom, P. E. Hopkins, A. Majumdar, R. Ramesh, and M. A. Zurbuchen, Nat. Mater. **13**, 168 (2014).
[43]G. Kresse and J. Hafner, Phys. Rev. B **47**, 558 (1993); **49**, 14251 (1994).
[44]G. Kresse and J. Furthmüller, Comput. Mat. Sci. **6**, 15 (1996).
[45]G. Kresse and J. Furthmüller, Phys. Rev. B **54**, 11169 (1996).
[46]G. Kresse and D. Joubert, Phys. Rev. B **59**, 1758 (1999).
[47]The views and conclusions contained in this document are those of the authors and should not be interpreted as representing the official policies. Either expressed or implied of the Defense Advanced Research Projects Agency; the U.S. Army Aviation and Missile Research, Development, and Engineering Center; or the U.S. Government.

Supplementary Information

Thermal conductivity of the n = 1 – 5 and 10 members of the $(SrTiO_3)_nSrO$ Ruddlesden-Popper superlattices

Molecular-Beam Epitaxy Thin-film Growth

Molecular beams of strontium and titanium were generated using a low-temperature effusion cell and a Ti-Ball™,[1] respectively. The fluxes of both elements were pre-calibrated using a quartz crystal microbalance. A more accurate flux calibration was done by following the reflection high-energy electron diffraction (RHEED) intensity oscillations.[2] Judging from the change of maximum/minimum intensity and the shape of oscillations, the shutter time needed for an absolute monolayer dose of each element is precisely determined. To grow $(SrTiO_3)_nSrO$ phases, both the stoichiometry and each monolayer absolute dose cannot be off by more than 1%. Each of the members in this series has different sequences of SrO and TiO_2 layers. We controlled the shutter ordering of strontium and titanium ions to match the layering sequence of the desired (001)-oriented $(SrTiO_3)_nSrO$ phases. All films were grown in an oxidant background pressure (O_2 + ~10% O_3) of 7×10^{-7} Torr at a substrate temperature of 850 °C (as measured by a thermocouple that is not in direct contact with the substrate); the true temperature of the substrate is closer to 750 °C.

X-Ray Diffraction Structural Characterization

To assess the quality and epitaxy of the 300 nm thick n = 2-5, and 10 $(SrTiO_3)_nSrO$ films grown on (100) $SrTiO_3$ and the 200 nm thick n = 1 $(SrTiO_3)_nSrO$ films grown on (100) LSAT, rocking curves in ω were measured shown in Fig. S1. All films were found to have full width at half maximums (FWHM) similar to the underlying substrates, indicative of high-quality epitaxial growth. From Fig. 1(a) in the main text the c-axis lattice constants of each member of the series, determined by Nelson-Riley analysis,[3] are found to be 12.63±0.03 Å, 20.29±0.01 Å, 28.16±0.02 Å, 35.84±0.03 Å, 43.68±0.02 Å, and 82.90±0.02 Å for the n = 1 (LSAT), 2, 3, 4, 5, and 10 phases, respectively. These values are similar to prior Ruddlesden-Popper films grown on (001) $SrTiO_3$ (Ref. 4) and (001) LSAT (Ref. 5).

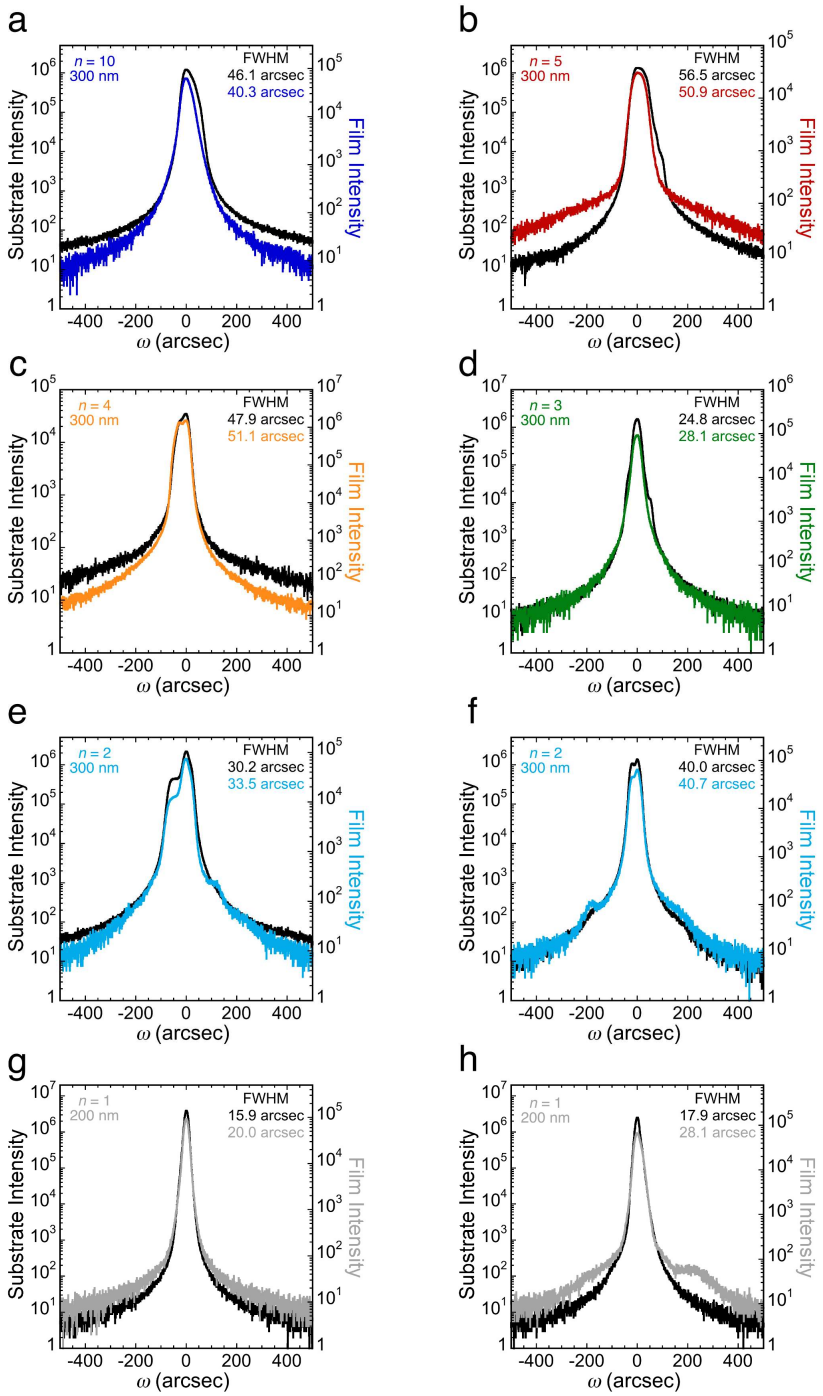

FIG. S1. ω rocking curves of the 300 nm thick n = 2-5, and 10 $(SrTiO_3)_nSrO$ films grown on (100) $SrTiO_3$ (a)-(f) and the 200 nm thick n = 1 $(SrTiO_3)_nSrO$ films grown on (100) LSAT (g) and (h). Superimposed XRD rocking curves of the 002 peaks of the $SrTiO_3$ or LSAT substrate (shown in black) and selected film peaks of the $(SrTiO_3)_nSrO$ n = 1 - 5, and 10 films: (a) n = 10 (00<u>42</u> peak, blue). (b) n = 5 (00<u>22</u> peak, red). (c) n = 4 (00<u>18</u> peak, orange). (d) n = 3 (00<u>14</u> peak, green). (e) n = 2 (00<u>10</u> peak, light blue). (f) n = 2 (00<u>10</u> peak, light blue). (**g**) n = 1 (006 peak, gray). (h) n = 1 (006 peak, gray). The full width at half maximum (FWHM) is given as a measure of crystalline quality for the substrate and film peaks.

Time-domain Thermoreflectance (TDTR) Measurements

Analysis of the TDTR data requires the heat capacities per unit volume of the thin film and the substrate. In cases where no published data of a material's heat capacity was available, we used the heat capacity of chemically and structurally similar phases to analyze the data. For $(SrTiO_3)_nSrO$, the temperature-dependent heat capacities were obtained by using the rule of mixtures to calculate the volumetric average of $SrTiO_3$ and SrO based on the index number *n*. Any systematic errors introduced by uncertainties in the heat capacity in TDTR are smaller than the other uncertainties in the experiment.

To measure TDTR at various temperature, samples were annealed at 300 °C for 30 minutes in order to remove any leftover organic residue on the surface of the sample. The samples were then coated with a 60–70 nm thick Al transducer layer using DC magnetron sputtering. The measurement was done using a single microscope objective lens, with a focused spot size of 10.7 μm. The power of the laser was controlled so that the steady-state temperature increase from the laser heating is less than 10 K. The thermal conductivity of the substrate was taken from the literature for LSAT[6] or was measured experimentally from single-crystal $SrTiO_3$ substrates.

Ab Initio Calculations

We performed fully *ab initio* calculations of the thermal conductivity in the Ruddlesden-Popper phases via the full solution of the Boltzmann transport equation (BTE)[7] within cubic anharmonicity. We obtained second- and third-order force constants via the temperature-dependent effective potential scheme by fitting the force constants to the forces produced during short *ab initio* molecular dynamics (AIMD) runs.[8] We adopted this approach since $SrTiO_3$ is dynamically stabilized in the cubic structure, and thus within the standard harmonic approximation the phonon spectrum features imaginary frequencies.[9] *Ab initio* molecular dynamics (AIMD) runs were performed for the total of 2000 time steps of 1 fs at 300 K by preparing 20 initial configurations drawn from a canonical distribution and

propagated for 100 time steps. This dataset features statistically independent set of forces and positions, appropriate for force constants fitting. The quality of each dataset was assessed by sampling different atomic configurations for force fitting and the results shows negligible differences between different samples. In VASP, the PBESol density functional[10] was adopted, with a 500 eV energy cutoff of the plane-wave expansion of the wavefunctions. The in-plane lattice constants of the simulated $(SrTiO_3)_nSrO$ phases were fixed to the corresponding substrate on which the material was grown, while the out-of-plane lattice constant (the *c*-axis of each $(SrTiO_3)_nSrO$ phase) was optimized. Primitive-cell calculations were performed with k-grid resolution of 6×6×6, while all AIMD runs were carried out at the Gamma point only on supercells ranging from 3×3×3 for $SrTiO_3$ to 3×3×1 for $Sr_5Ti_4O_{13}$. The distance cutoffs for second- and third-order force constants were 5 A and 4.5 A, respectively, and we neglected electrostatic long-range contributions to the phonons, *i.e.*, the spectrum does not feature splitting of the longitudinal and transverse optical phonons. We further assumed that the force constants are only weakly temperature-dependent in the range relevant for the experimental observations, and thus we used resultant force constants to calculate the thermal conductivity in the 150-500 K range for comparison with the experimental data. The phonon mean free path for a given compound was estimated as the 50% point of the thermal conductivity accumulation function.

References

1. C. D. Theis and D. G. Schlom, J. Vac. Sci. Technol. A **14**, 2677 (1996).
2. J. H. Haeni, C. D. Theis, and D. G. Schlom, J. Electroceram. **4**, 385 (2000).
3. J. B. Nelson and D. P. Riley, Proc. Phys. Soc. London **57**, 160 (1945).
4. J. H. Haeni, C. D. Theis, D. G. Schlom, W. Tian, X. Q. Pan, H. Chang, I. Takeuchi, and X.-D. Xiang, Appl. Phys. Lett. **78**, 3292 (2001).

5. C. H. Lee, N. J. Podraza, Y. Zhu, R. F. Berger, S. Shen, M. Sestak, R. W. Collins, L. F. Kourkoutis, J. A. Mundy, H. Q. Wang, Q. Mao, X. X. Xi, L. J. Brillson, J. B. Neaton, D. A. Muller, and D. G. Schlom, Appl. Phys. Lett. **102** 122901 (2013).

6. J. Hidde, C. Guguschew, S. Ganschow, D. Klimm, J. Alloy Compd. **738**, 415 (2018).

7. A. Ward, D. A. Broido, D. A. Stewart, and G. Deinzer, Phys. Rev. B. **80**, 125203 (2009).

8. O. Hellman and I. A. Abrikosov, Phys. Rev. B **88**, 144301 (2013).

9. J.-J. Zhou, O. Hellman, and M. Bernardi, Phys. Rev. Lett. **121**, 226603 (2018).

10. G. I. Csonka, J. P. Perdew, A. Ruzsinszky, P. H. T. Philipsen, S. Lebègue, J. Paier, O. A. Vydrov, and J. G. Ángyán, Phys. Rev. B **79**, 155107 (2019).